The Canadian Mineralogist
Vol. 57, pp. 637-646 (2019)
DOI: 10.3749/canmin.1900025

NICKELTYRRELLITE, $CuNi_2Se_4$, A NEW MEMBER OF THE SPINEL SUPERGROUP FROM EL DRAGÓN, BOLIVIA

HANS-JÜRGEN FÖRSTER[§]

Helmholtz Centre Potsdam German Research Centre for Geosciences GFZ D - 14473 Potsdam, Germany

CHI MA

Division of Geological and Planetary Sciences, California Institute of Technology, Pasadena, California 91125, USA

GÜNTER GRUNDMANN

Eschenweg 6, D-32760 Detmold, Germany

LUCA BINDI

Dipartimento di Scienze della Terra, Università degli Studi di Firenze, Via G. La Pira 4, I-50121 Firenze, Italy

CHRISTOPHER J. STANLEY

Department of Earth Sciences, Natural History Museum, Cromwell Road, London SW7 5BD, United Kingdom

ABSTRACT

Nickeltyrrellite, ideally $CuNi_2Se_4$, is a new selenide species from the El Dragón mine, Department of Potosí, Bolivia. It most frequently occurs as anhedral to subhedral grains (up to 20 μm in size) in association with cerromojonite, klockmannite, clausthalite, and penroseite, forming fracture fillings in pre-existing krut'aite–penroseite solid solutions. Nickeltyrrellite is non-fluorescent, black, and opaque with a metallic luster and black streak. It is brittle, with an irregular fracture and no obvious cleavage and parting. In plane-polarized incident light, nickeltyrrellite is cream to pale pinkish, displaying no internal reflections. Between crossed polarizers, it is isotropic. The reflectance values in air for the COM standard wavelengths are 45.9 (470 nm), 47.6 (546 nm), 48.1 (589 nm), and 49.8 (650 nm). Electron-microprobe spot analyses ($n = 28$) of the grain populations used for the EBSD study yielded a mean composition of Cu 13.01, Fe 0.27, Co 6.66, Ni 16.98, S 1.04, Se 61.91, total 99.87 wt.%. The empirical formula, normalized to 7 *apfu*, is $Cu_{1.00}(Ni_{1.42}Co_{0.56}Fe_{0.02})_{\Sigma 2.00}(Se_{3.84}S_{0.16})_{\Sigma 4.00}$. The ideal formula is $CuNi_2Se_4$, which requires (in wt.%) Cu 12.79, Ni 23.63, Se 63.58, total 100. EBSD patterns reveal nickeltyrrellite as cubic, space group $Fd\bar{3}m$, with $a = 9.99$ Å, $V = 997.0$ Å^3, $Z = 8$. The calculated density is 7.36 g cm^{-3}. It formed in response to alteration of quijarroite + hansblockite + watkinsonite + clausthalite + penroseite aggregates by oxidizing, low-*T*, Cu-Ni-Co-Pb-bearing fluids at a fSe_2/fS_2 ratio greater than unity. Nickeltyrrellite is a new selenide belonging to the tyrrellite subgroup of the spinel supergroup. The new species has been approved by the IMA-CNMNC (2018-110) and is named for constituting the Ni-analogue of tyrrellite.

Keywords: new mineral, nickeltyrrellite, tyrrellite, chemical composition, EBSD, spinel supergroup, El Dragón, Bolivia.

INTRODUCTION

The ore mineralization at El Dragón, Province of Antonio Quijarro, in the Andes of Bolivia is the most spectacular occurrence of Se-bearing minerals known today. Although volumetrically very minor, a total of 29 selenides and selenates have been detected to date. The most recently discovered Se-species encompass eldragónite, $Cu_6BiSe_4(Se_2)$ (Paar *et al.* 2012); favreauite, $PbBiCu_6O_4(SeO_3)_4(OH)\cdot H_2O$ (Mills *et al.*

§ *Corresponding author e-mail address*: forhj@gfz-potsdam.de

2014); alfredopetrovite, $Al_2(Se^{4+}O_3)_3 \cdot 6H_2O$ (Kampf *et al*. 2016); grundmannite, $CuBiSe_2$ (Förster *et al*. 2016a); quijarroite, $Cu_6HgPb_2Bi_4Se_{12}$ (Förster *et al*. 2016b); hansblockite, $(Cu,Hg)(Bi,Pb)Se_2$ (Förster *et al*. 2017); and cerromojonite, $CuPbBiSe_3$ (Förster *et al*. 2018). El Dragón also hosts the most recently IMA-CNMNC approved selenide, luxembourgite, $AgCuPbBi_4Se_8$ (Philippo *et al*. 2019) (*cf*. Grundmann & Förster 2017, their Table 3, #6).

This paper describes a new species in the Cu–Co–Ni–Se system, nickeltyrrellite, ideally $CuNi_2Se_4$, from El Dragón. The new mineral and its name have been approved by the Commission on New Minerals, Nomenclature, and Classification (CNMNC) of the IMA, proposal 2018–110. The holotype polished section is housed in the collections of the Natural History Museum, London, catalogue number BM 2018, 19. Cotype material is stored at the Mineralogical State Collection Munich–Museum Reich der Kristalle, inventory number MSM 73587. The name of the mineral indicates that it is the Ni-analogue of tyrrellite, $CuCo_2Se_4$ (Robinson & Brooker 1952, Harris 1970).

Background on Geology

The geology and origin of the El Dragón selenide occurrence were comprehensively described by Grundmann & Förster (2017). The mine is located in southwestern Bolivia, in the Cordillera Oriental, some 30 km southwest of Cerro Rico de Potosí. The abandoned mine is located at 19° 49′ 23.90″ S (latitude), 65° 55′ 00.60″ W (longitude), at an altitude of 4160 m above sea level. The almost vertical ore vein is located in the center of a 1.5 m-wide shear zone penetrating a series of thinly stratified, pyrite-rich black shales and reddish-grey, hematite-bearing siltstones of probably Devonian age. The selenium mineralization consisted of a single vein of small longitudinal extension (maximum 15 m-long), ranging mostly from 0.5 to 2 cm in thickness.

Appearance

Nickeltyrrellite occurs within two texturally different mineral assemblages, which are interpreted as pseudomorphs after quijarroite/hansblockite/watkinsonite/clausthalite/type-I cerromojonite/penroseite intersertal aggregates (Förster *et al*. 2016a, 2016b, 2017, 2018).

Type-I nickeltyrrellite (inclusion-free grain size ≤ 20 μm) is anhedral and occurs inside and/or at the margin of fine-grained granular or myrmekitic aggregates predominantly composed of penroseite, which generally show a finely branched network of shrinkage cracks (Fig. 1).

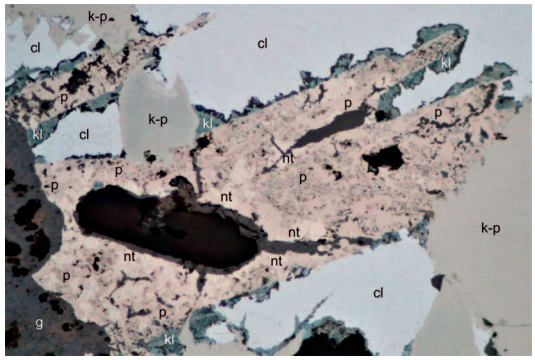

FIG. 1. Type-I nickeltyrrellite (nt) in association with penroseite (p), klockmannite (kl), and clausthalite (cl). Reflected light digital image. Width 200 μm.

Type-II nickeltyrrellite (inclusion-free grain-size ≤ 20 μm) is sub- to anhedral, rarely forms subhedral crystals (cube-octahedra), and crystallized inside and/or at the margin of lath-shaped or acicular type-II cerromojonite aggregates (Fig. 2), which may be intimately (sub-parallel) intergrown with relict quijarroite/hansblockite/watkinsonite and newly formed clausthalite and (according to energy-dispersive electron-microprobe analysis) two new Cu-(Ag)-Hg-Pb-Bi selenides (Förster *et al*. 2018).

Physical and Optical Properties

Nickeltyrrellite is non-fluorescent, black, and opaque with a metallic luster and black streak. It is brittle with an irregular fracture and no obvious parting and cleavage. Vickers hardness and density could not be measured because of the small grain size. Density calculated from EBSD data is 7.36 g/cm^3.

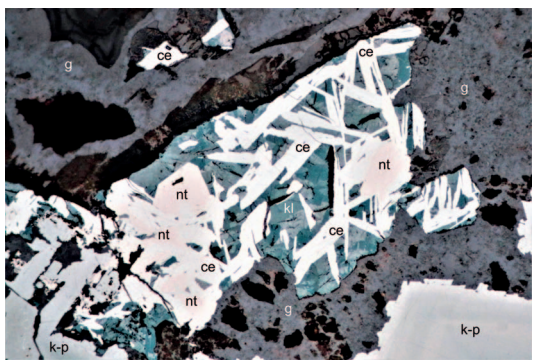

FIG. 2. Type-II nickeltyrrellite (nt) in association with type-II cerromojonite (ce) and klockmannite (kl). g = goethite, k-p = krut'aite–penroseite solid solution. Reflected light digital image. Width 200 μm.

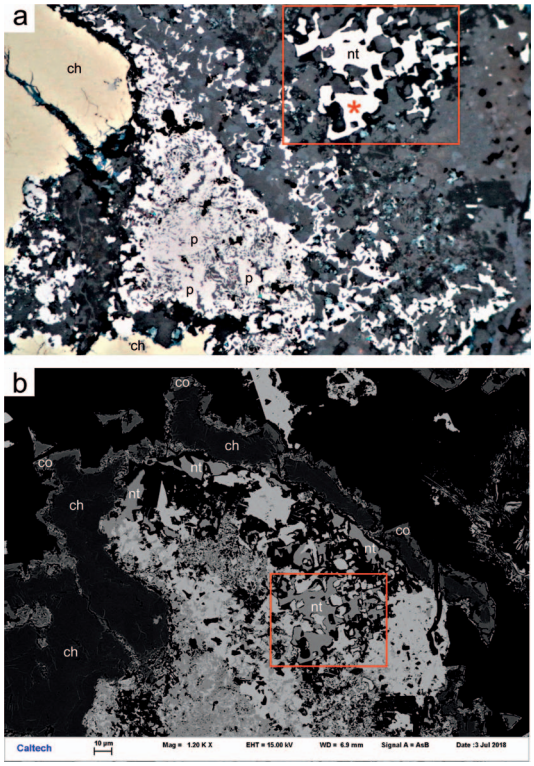

FIG. 3. (a) Reflected light digital image (width 200 μm) and (b) corresponding SEM-BSE image of an altered type-I nickeltyrrellite (nt)/penroseite (p) aggregate mantled by chalcopyrite (ch) and covellite (co). The red rectangle encloses population 62/area 2a of nickeltyrrellite grains analyzed for compositions (*cf.* Tables 2 and 3). The red asterisk marks one of the two grains studied for crystal structure.

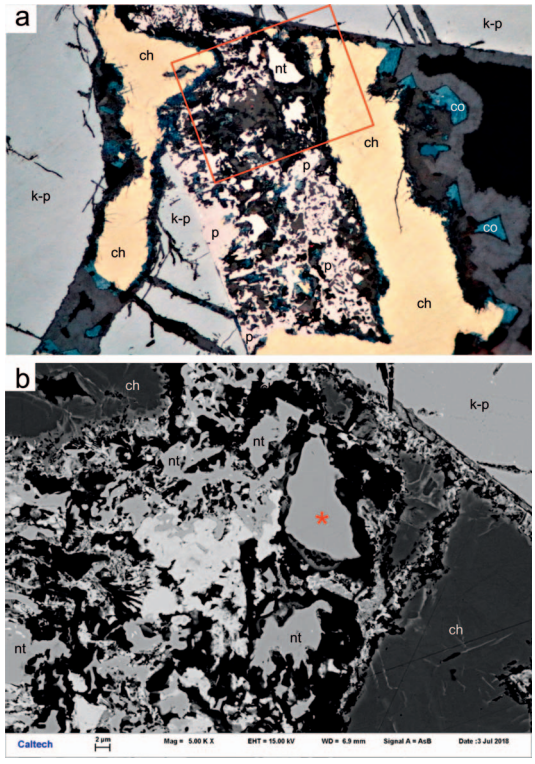

FIG. 4. (a) Reflected light digital image (width 200 μm) and (b) corresponding SEM-BSE image of another altered type-I nickeltyrrellite (nt)/penroseite (p) assemblage overgrown by chalcopyrite (ch), covellite (co), and other unspecified alteration minerals. The red rectangle encloses population 62/area 2b of nickeltyrrellite grains analyzed for compositions (*cf.* Tables 2 and 3). The red asterisk marks the second grain studied for crystal structure. k-p = krut'aite–penroseite solid solutions.

In plane-polarized incident light, nickeltyrrellite is cream against chalcopyrite, covellite, penroseite, krut'aite–penroseite, and the unidentified alteration products (*cf.* Figs. 3 and 4). Nickeltyrrellite is pale pinkish against cerromojonite in the assemblage with klockmannite, penroseite, clausthalite, and krut'aite–penroseite (*cf.* Fig. 2). With crossed polarizers, nickeltyrrellite is isotropic.

Quantitative reflectance data were obtained in air relative to a Zeiss WTiC standard using a J and M TIDAS diode array spectrometer attached to a Zeiss Axiotron microscope. Reflectance values were measured in air from an area of 8 by 8 μm (asterisk in Fig. 4b), from which the chemical composition and EBSD data were obtained. The results are listed in Table 1.

CHEMICAL COMPOSITION

The nickeltyrrellite grains were routinely analyzed for concentrations of Cu, Ag, Pb, Hg, Fe, Co, Ni, As, Sb, Bi, S, and Se. Quantitative chemical analyses were conducted in WDS mode, using a JEOL JXA-8230 electron probe X-ray microanalyzer at Deutsches GeoForschungsZentrum GFZ, Potsdam, Germany. The probe was operated at 20 kV, 20 nA, and 1–2 μm beam size. The counting time on peak was 20–40 s, with half that time on background on both sides of the peak. The following emission lines and analyzing crystals (in parentheses) were used: Cu – *K*α (LIFL); Fe – *K*α (LIFH); Co – *K*α (LIFL); Ni – *K*α (LIFL); S – *K*α (PETJ); Se – Lα (TAPH). The CITZAF routine in the JEOL software, which is based on the φ(ρZ)

TABLE 1. REFLECTANCE DATA FOR NICKELTYRRELLITE

λ (nm)	*R* (%)	λ (nm)	*R* (%)
400	42.1	640	49.7
420	43.3	660	50.1
440	44.4	680	50.5
460	45.4	700	51.0
480	46.2		
500	46.7	Commission on	
520	47.1	Ore Mineralogy (COM)	
		wavelengths	
540	47.5		
560	47.8	470	45.9
580	48.3	546	47.6
600	48.8	589	48.1
620	49.9	650	49.8

method (Armstrong 1995), was used for data processing.

Compositional data (28 spots) acquired for the two grain type-II nickeltyrrellite populations from the holotype section subjected to structural study (*cf.* Figs. 3 and 4) are compiled in Table 2 and also listed in Table 3 (62/areas 2a and 2b). The grains are homogeneous within analytical error but are slightly variable in composition in terms of Ni/Co and Se/S ratios. The empirical formula is $Cu_{1.00}(Ni_{1.42}Co_{0.56}Fe_{0.02})_{\Sigma 2.00}(Se_{3.84}S_{0.16})_{\Sigma 4.00}$ (based on 7 atoms *pfu*). The ideal formula is $CuNi_2Se_4$, which requires (in wt.%) Cu 12.79, Ni 23.63, Se 63.58, total 100.

Altogether, 75 spots were analyzed on both type-I and type-II nickeltyrrellite in three samples from El Dragón (Table 3). Detected components display the following ranges of concentrations (in wt.%): Cu 11.30–13.38; Fe 0.05–1.24; Co 1.90–9.12; Ni 14.09–22.24; S 0.03–2.18; Se 60.22–64.23. The mean formula (based on 7 atoms *pfu*) derived from the 75 spots is $Cu_{0.97}(Ni_{1.52}Co_{0.47}Fe_{0.03})_{\Sigma 2.02}(Se_{3.93}S_{0.08})_{\Sigma 4.01}$.

Notably, grains from two areas (62/area 1 and 14/area 2a) are too low in Cu to completely fill the Cu position. It is likely that other cations (Fe, Co, and/or Ni) have entered this position (see Discussion section).

EBSD Study

Conventional single-crystal X-ray and powder-diffraction studies could not be carried out because of the small crystal size. Alternatively, electron backscatter diffraction (EBSD) analyses of two fragments (Figs. 3 and 4) were performed using an HKL EBSD system on a ZEISS 1550VP Field-Emission SEM at Caltech, operated at 20 kV and 6 nA in focused-beam mode with a 70° tilted stage and in a variable pressure mode (25 Pa). The focused electron beam was several nanometers in diameter. The spatial resolution for diffracted backscatter electrons was ~30 nm. The EBSD system was calibrated using a single-crystal silicon standard. The determination of the cell parameters and suggestions of the possible crystal structure were obtained by matching the experimental EBSD patterns with structures of Cu-Ni-S, Cu-Co-Se, and Ni-Se phases.

The EBSD patterns can only be indexed by the $Fd\bar{3}m$ spinel-type structure and give a best fit to the tyrrellite $[Cu(Co_{0.68}Ni_{0.32})_2Se_4]$ cell from Yang *et al.* (2007) (Fig. 5), with a mean angular deviation of 0.45–0.56°, revealing the following cubic unit-cell parameters: $a = 9.99$ Å, $V = 997.0$ Å^3, and $Z = 8$.

Discussion

Relation to other species

The new mineral described here is the Ni-analogue of tyrrellite, $CuCo_2Se_4$, which is itself the Se-analogue of fletcherite, $CuNi_2S_4$ (Craig & Carpenter 1977). The scientific rationale for preferring the name nickeltyrrellite instead of selenofletcherite is explained below.

As pointed out in the recent classification of the spinel supergroup (Bosi *et al.* 2019), properly classifying Cu-bearing chalcospinels is quite challenging (Table 4). This is mainly due to the fact that confidence

TABLE 2. CHEMICAL COMPOSITION (wt.%) OF NICKELTYRRELLITE STUDIED FOR STRUCTURE

Constituent	Mean	Range	1δ	EMP Standard
Cu	13.01	12.71–13.38	0.16	chalcopyrite
Fe	0.27	0.05–1.04	0.29	chalcopyrite
Co	6.66	3.10–8.83	1.86	cobaltite
Ni	16.98	14.36–20.10	1.67	pentlandite
S	1.04	0.03–2.18	0.69	chalcopyrite
Se	61.91	60.22–63.62	1.04	synthetic Bi_2Se_3
Total	99.87	98.97–100.82	0.46	

1δ = standard deviation.

TABLE 3. MEAN COMPOSITION (wt.%) AND FORMULA PROPORTIONS OF SIX GRAIN POPULATIONS OF NICKELTYRRELLITE FROM THREE SAMPLES

	62/area 2a		62/area 2b		62/area 1		123GG3/area 2c		14/area 1		14/area 2a	
	mean (21)	1δ	mean (7)	1δ	mean (8)	1δ	mean (14)	1δ	mean (9)	1δ	mean (16)	1δ
Cu (wt.%)	13.03	0.17	12.93	0.10	11.56	0.02	12.95	0.20	12.62	0.14	11.70	0.26
Fe	0.25	0.34	0.33	0.04	0.82	0.20	0.31	0.27	0.35	0.33	0.31	0.25
Co	7.67	0.62	3.64	0.34	2.41	0.01	8.31	0.63	4.29	0.49	3.88	0.87
Ni	16.11	0.74	19.58	0.46	21.51	0.16	15.13	0.53	18.86	0.72	20.30	0.59
S	1.38	0.42	0.05	0.03	0.12	0.04	0.40	0.14	0.18	0.12	0.14	0.08
Se	61.43	0.66	63.37	0.26	63.63	0.32	63.05	0.28	63.08	0.33	63.25	0.25
sum	99.86	0.48	99.90	0.43	100.04	0.28	100.16	0.34	99.38	0.72	99.57	0.50
Cu (*apfu*)	1.00	0.01	1.01	0.01	0.90	0.00	1.00	0.01	0.99	0.01	0.92	0.02
Fe	0.02	0.03	0.03	0.00	0.07	0.02	0.03	0.02	0.03	0.03	0.03	0.02
Co	0.63	0.05	0.31	0.03	0.20	0.00	0.70	0.05	0.36	0.04	0.33	0.07
Ni	1.34	0.06	1.66	0.04	1.82	0.01	1.27	0.04	1.60	0.06	1.72	0.05
S	0.21	0.06	0.01	0.00	0.02	0.01	0.06	0.02	0.03	0.02	0.02	0.01
Se	3.80	0.06	3.98	0.01	3.99	0.01	3.94	0.03	3.99	0.04	3.98	0.03

1δ = 1δ standard deviation; numbers in parentheses indicate the number of spots used for mean calculation. Formula proportions calculated according to 7 atoms *pfu*.

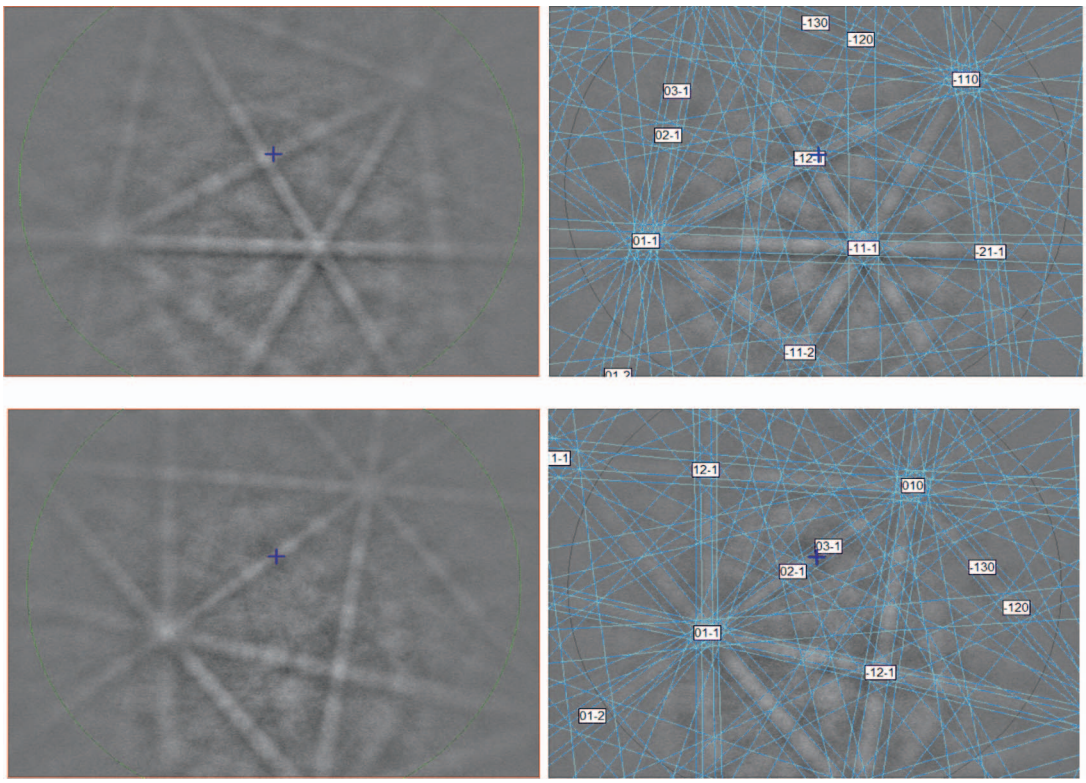

FIG. 5. (left) EBSD patterns of two $CuNi_2Se_4$ crystals (*cf.* Figs. 3 and 4) with different orientations and (right) the patterns indexed with the $Fd\bar{3}m$ tyrrellite structure.

TABLE 4. CLASSIFICATION OF THE S/SE SPECIES IN THE SPINEL SUPERGROUP

Thiospinel group			
carrollite subgroup (1–3.5)	A^{1+}	$B^{3.5+}$	X
carrollite	Cu	Co_2	S_4
cuproiridsite	Cu	$(Ir^{3+}Ir^{4+})$	S_4
cuprokalininite	Cu	$(Cr^{3+}Cr^{4+})$	S_4
fletcherite	Cu	Ni_2	S_4
florensovite	Cu	$(Cr^{3+}{}_{1.5}Sb^{5+}{}_{0.5})$	S_4
malanite	Cu	$(Ir^{3+}Pt^{4+})$	S_4
rhodostannite	Cu	$(Fe^{2+}{}_{0.5}Sn^{4+}{}_{1.5})$	S_4
toyohaite	Ag	$(Fe^{2+}{}_{0.5}Sn^{4+}{}_{1.5})$	S_4
linnaeite subgroup (2–3)	A^{2+}	B^{3+}	X
cadmoindite	Cd	In_2	S_4
cuprorhodsite	$(Cu^{+}{}_{0.5}Fe^{3+}{}_{0.5})$	Rh_2	S_4
daubréelite	Fe	Cr_2	S_4
greigite	Fe	Fe_2	S_4
indite	Fe	In_2	S_4
joegoldsteinite	Mn	Cr_2	S_4
kalininite	Zn	Cr_2	S_4
linnaeite	Co	Co_2	S_4
polydymite	Ni	Ni_2	S_4
siegenite	Co	Ni_2	S_4
violarite	Fe	Ni_2	S_4
xingzhongite	Pb	Ir_2	S_4
Selenospinel group			
tyrrellite subgroup (1–3.5)	A^{1+}	$B^{3.5+}$	X
tyrrellite	Cu	$(Co,Ni)_2$	Se_4
nickeltyrrellite	**Cu**	**Ni_2**	**Se_4**
bornhardtite subgroup (2–3)	A^{2+}	B^{3+}	X
bornhardtite	Co	Co_2	Se_4
trüstedtite	Ni	Ni_2	Se_4

about the charge of ions in these minerals is lacking. Although Cu is usually considered to be monovalent in sulfides, carrollite ($CuCo_2S_4$) has been traditionally considered a 2–3 species, $Cu^{2+}Co^{3+}{}_2(S^{2-})_4$ (*e.g.*, Charnock *et al.* 1990). Pattrick *et al.* (2008) and Buckley *et al.* (2009) studied the Co charge in carrollite spectroscopically and obtained contrasting results. Pattrick *et al.* (2008) suggested a Co charge between 2+ and 3+, giving rise to the formula $Cu^{+}(Co^{2+}Co^{3+})(S^{1.5-})_4$, whereas Buckley *et al.* (2009) proposed low-spin Co^{3+} with a charge for S only 12.5% less negative than 2–, which leads to $Cu^{+}Co^{3+}{}_2(S^{1.75-})_4$. Concerning fletcherite, $CuNi_2S_4$, no information on the crystal structure and the formal ions charge is available. For tyrrellite, $Cu(Co,Ni)_2Se_4$, it has been suggested that Cu is monovalent, and Co or Ni exhibit a charge >3+ (Yang *et al.* 2007 and references therein).

To classify chalcospinels, Bosi *et al.* (2019) assumed that the oxidation states of anions (S and Se) and Cu are 2– and 1+, respectively. This implies the presence of Co^{3+}, Co^{4+}, Ni^{3+}, and Ni^{4+}, leading to an overall charge for the octahedral cation of 3.5+. As a result, carrollite, fletcherite, and tyrrellite fall into the subgroup 1–3.5 (Bosi *et al.* 2019). Tyrrellite has been considered as an isolated member of a potential "tyrrellite subgroup", given the fact that the minimum requirement to have a mineral subgroup is that it contains at least two species (Mills *et al.* 2009). With the discovery of nickeltyrrellite, the "tyrrellite subgroup" gains its proper status.

The mineral described here compositionally resembles "unnamed phase $CuNi_2Se_4$", described from El Dragón by Grundmann & Förster (2017). In Figure 14 of that paper, penroseite was regrettably confused with the "unnamed phase $CuNi_2Se_4$", which turned out to be type-I nickeltyrrellite which, in this case, partially replaces penroseite.

To display the presently known spread in composition of the nickeltyrrellite–tyrrellite solid-solution series, data for nickeltyrrellite from El Dragón and

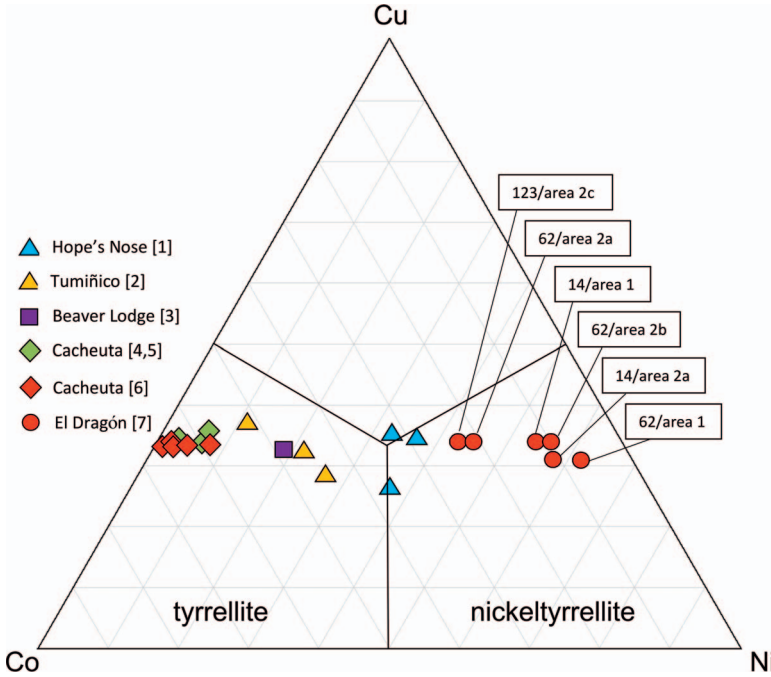

FIG. 6. Co–Ni–Cu ternary diagram (mole%) of the system $(Co,Ni,Cu)_3Se_4$. References: 1 – Stanley *et al*. (1990), 2 – Paar *et al*. (2002), 3 – Criddle & Stanley (1986), 4, 5 – Paar *et al*. (1996, 2016), 6 – Grundmann & Förster (2018), 7 – This work. Designation of the six areas showing data from El Dragón correspond to the mean compositions in Table 3.

published information on tyrrellite were plotted in a Cu–Co–Ni ternary diagram of the system $CuCu_2Se_4$–$CuCo_2Se_4$–$CuNi_2Se_4$ (Fig. 6). This plot indicates that miscibility between tyrrellite and nickeltyrrellite is most likely complete. Although most of the analyses from Hope's Nose, UK, published by Stanley *et al*. (1990), fall in the tyrrellite field, the most Ni-rich spot analysis yields the formula (based on 7 atoms *pfu*) $Cu_{1.03}(Ni_{1.10}Co_{0.85})_{\Sigma 1.95}Se_{4.02}$ and, consequently, is classified as nickeltyrrellite.

Origin

Nickeltyrrellite from El Dragón is a late-stage mineral deposited during stage III ("fracture fillings") as defined by Grundmann & Förster (2017) (Fig. 7). It formed in response to the alteration of quijarroite-hansblockite-watkinsonite-clausthalite-penroseite ± type-I cerromojonite aggregates by low-*T*, late-stage Cu-Co-Ni-Pb-Se-bearing oxidizing fluids. Type-I and type-II nickeltyrrellite-containing mineral assemblages were deposited in the interstices or at the surface of fractured krut'aite–penroseite solid solutions (Figs. 8–10). They precipitated during the same event, but from differently textured "mother" aggregates. The precursors of type-I nickeltyrrellite are fine-grained granular or myrmekitic aggregates, whereas type-II nickeltyrrellite is related to porous aggregates relatively more abundant in open spaces between the pre-existing lath-shaped or acicular grains of Cu-Ag-Hg-Pb-Bi selenides. These open spaces permitted type-II nickeltyrrellite to grow more freely and to locally develop crystal shapes (*cf*. Fig. 2). Associated type-II cerromojonite represents the alteration product of the Bi selenides, with Ag and Hg being lost to the fluid phase. Overprinting may have been intense, as the precursor Bi selenides were completely dissolved, and the aggregates transformed into the assemblage nickeltyrrellite + penroseite + clausthalite + klockmannite (*cf*. Fig. 1).

Dissolution and partial replacement of Ni-Co-rich rim zones of angular krut'aite–penroseite solid solutions (k-p) by late clausthalite or penroseite (*cf*. Figs. 8 and 9) provide evidence that k-p grain surfaces underwent local corrosion to release Cu, Ni, and Co, which were trapped by newly grown nickeltyrrellite and, probably, penroseite. Whether penroseite and nickeltyrrellite in association always formed simultaneously could not be confidently answered, since this penroseite is chemically indistinguishable from the "old" penroseite included in the precursor Bi-selenide aggregates. Subsequent alteration of nickeltyrrellite,

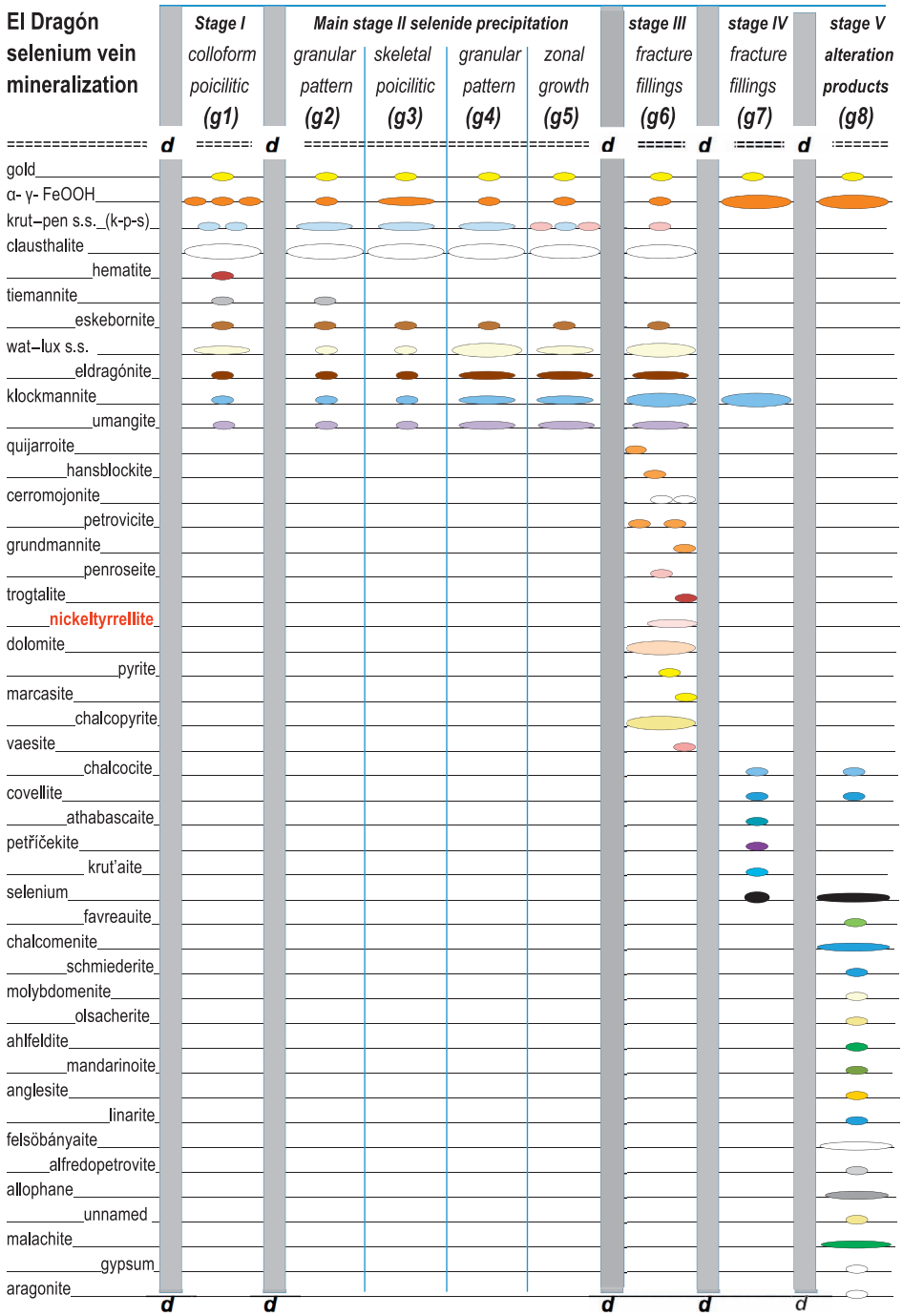

FIG. 7. Paragenetic sequence and crystallization/deformation diagram for the El Dragón selenium mineralization (after Grundmann & Förster 2017). krut = krut'aite, pen = penroseite, wat = watkinsonite, lux = luxembourgite, s.s. = solid solutions.

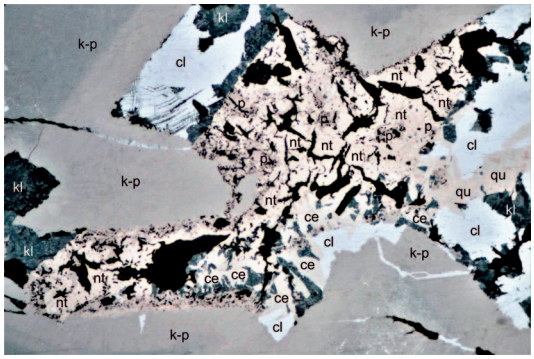

FIG. 8. Type-II nickeltyrrellite in association with penroseite (p), klockmannite (kl), type-II cerromojonite (ce), and clausthalite (cl), interpreted as a pseudomorph after a formerly angular network-like intersertal texture of quijarroite (qu), hansblockite, type-I cerromojonite, and watkinsonite. A replacement relic of quijarroite and penroseite surrounded by clausthalite is shown on the right side of the image. k-p = krut'aite–penroseite solid solution. Reflected light digital image. Width 500 μm.

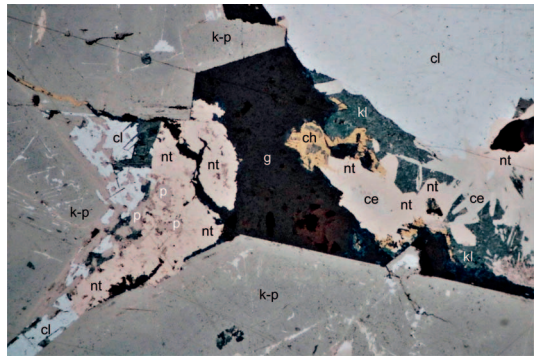

FIG. 10. (left) Partial replacement of Ni-Co-rich rim zones of angular krut'aite–penroseite solid solutions (k-p) by late clausthalite (cl) provides evidence that the concave surfaces have undergone corrosion to release Cu, Ni, and Co, subsequently trapped by type-II nickeltyrrellite (nt) and possibly penroseite (p). (right) Alteration of a type-II nickeltyrrellite + cerromojonite + klockmannite aggregate by chalcopyrite (ch). g = goethite. Reflected light digital image. Width 200 μm.

cerromojonite, and klockmannite assemblages by late chalcopyrite, covellite, and goethite caused strong fretting that significantly reduced the grain-size of nickeltyrrellite and penroseite (*cf.* Fig. 10).

Inferences regarding the physico-chemical environment of formation of nickeltyrrellite could be made from the type of Cu selenide with which it is associated (clausthalite and penroseite have much larger stability fields). Its occurrence together with klockmannite implies high selenium fugacities above values defined by the umangite–klockmannite univariant reaction, but below those required to precipitate krut'aite. Assuming a temperature of 100 °C (which is probably too high) and an elevated oxygen fugacity defined by the magnetite–hematite buffer, this paragenetic relation is consistent with a range of log f_{Se2} between −14.4 and −11.6 (Simon *et al.* 1997). The absence of krut'aite and sulfides (chalcopyrite, pyrite) restricts the maximum log f_{S2} to roughly −19.

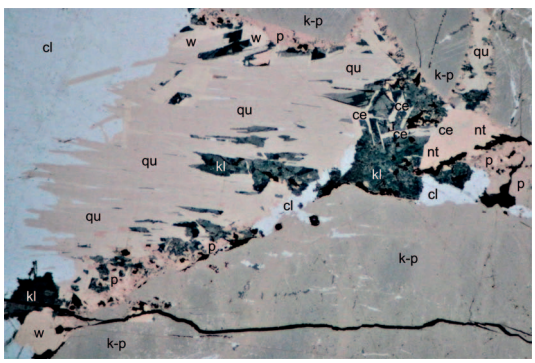

FIG. 9. Aggregate of penroseite-poor, parallel crystallized Cu-Hg-Pb-Bi selenides partially altered to late klockmannite (kl), penroseite (p), type II cerromojonite (ce), and type-II nickeltyrrellite (at right). cl = clausthalite, qu = quijarroite, w = watkinsonite, k-p = krut'aite–penroseite solid solution. Reflected light digital image. Width 500 μm.

ACKNOWLEDGMENTS

We wish to thank Oona Appelt (GFZ Potsdam) for her help with the electron microprobe work. C.J.S. acknowledges Natural Environment Research Council grant NE/M010848/1 Tellurium and Selenium Cycling and Supply. Comments of Giovanni B. Andreozzi and an anonymous reviewer are appreciated.

REFERENCES

ARMSTRONG, J.T. (1995) *CITZAF*: A package of correction programs for the quantitative electron microbeam X-ray-analysis of thick polished materials, thin films, and particles. *Microbeam Analysis* **4**, 177–200.

BOSI, F., BIAGIONI, C., & PASERO, M. (2019) Nomenclature and classification of the spinel supergroup. *European Journal of Mineralogy* **31**, 183–192.

BUCKLEY, A.N., SKINNER, W.M., HARMER, S.L., PRING, A., & FAN, L.-J. (2009) Electronic environments in carrollite, $CuCo_2S_4$, determined by soft X-ray photoelectron and absorption spectroscopy. *Geochimica et Cosmochimica Acta* **73**, 4452–4467.

Charnock, K., Garner, C.D., Pattrick, R.A.D., & Vaughan, D.J. (1990) An EXAFS study of thiospinel minerals. *American Mineralogist* **75**, 247–255.

Craig, J.R. & Carpenter, A.B. (1977) Fletcherite, $Cu(Ni,Co)_2S_4$, a new thiospinel from the Viburnum Trend (new lead belt), Missouri. *Economic Geology* **72**, 480–486.

Criddle, A.J. & Stanley, C.J. (1986) *The Quantitative Data File for Ore Minerals*. 2nd Edition, British Museum of Natural History, London, England, 274–275.

Förster, H.-J., Bindi, L., & Stanley, C.J. (2016a) Grundmannite, $CuBiSe_2$, the Se-analogue of emplectite: A new mineral from the El Dragón mine, Potosí, Bolivia. *European Journal of Mineralogy* **28**, 467–477.

Förster, H.-J., Bindi, L., Grundmann, G., & Stanley, C.J. (2016b) Quijarroite, $Cu_6HgPb_2Bi_4Se_{12}$, a new selenide from the El Dragón mine, Bolivia. *Minerals* **6**, 11 pp.

Förster, H.-J., Bindi, L., Stanley, C.J., & Grundmann, G. (2017) Hansblockite, $(Cu,Hg)(Bi,Pb)Se_2$, the monoclinic polymorph of grundmannite: A new mineral from the Se mineralization at El Dragón (Bolivia). *Mineralogical Magazine* **81**, 629–640.

Förster, H.-J., Bindi, L., Grundmann, G., & Stanley, C.J. (2018) Cerromojonite, $CuPbBiSe_3$, a new member of the bournonite group. *Minerals* **8**, 14 pp.

Grundmann, G. & Förster, H.-J. (2017) Origin of the El Dragón selenium mineralization, Quijarro Province, Potosí, Bolivia. *Minerals* **7**, 23 pp.

Grundmann, G. & Förster, H.-J. (2018) The Sierra de Cacheuta vein-type Se mineralization, Mendoza Province, Argentina. *Minerals* **8**, 22 pp.

Harris, D.C. (1970) New data on tyrrellite. *Canadian Mineralogist* **10**, 731–736.

Kampf, A.R., Mills, S.J., Nash, B.P., Thorne, B., & Favreau, G. (2016) Alfredopetrovite: a new selenite mineral from the El Dragón mine. *European Journal of Mineralogy* **28**, 479–484.

Mills, S.J., Hatert, F., Nickel, E.H., & Ferraris, G. (2009) The standardisation of mineral group hierarchies: Application to recent nomenclature proposals. *European Journal of Mineralogy* **21**, 1073–1080.

Mills, S.J., Kampf, A.R., Christy, A.G., Housley, R.M., Thorne, B., Chen, Yu-Sheng, & Steele, I.M. (2014) Favreauite, a new selenite mineral from the El Dragón mine, Bolivia. *European Journal of Mineralogy* **26**, 771–781.

Paar, W.H., Sureda, R.J., & de Brodtkorb, M.K. (1996) Mineralogía de los yaciminientos de selenio en La Rioja, Argentina. Krutaita, tyrrellita y trogtalita de Los Llantenes. *Revista de la Asociación Geológica Argentina* **51**, 304–312.

Paar, W.H., Topa, D., Roberts, A.C., Criddle, A.J., Amann, G., & Sureda, R.J. (2002) The new mineral species brodtkorbite, Cu_2HgSe_2, and the associated selenide assemblage from Tumiñico, Sierra de Cacho, La Rioja, Argentina. *Canadian Mineralogist* **40**, 225–237.

Paar, W.H., Cooper, M.A., Moëlo, Y., Stanley, C.J., Putz, H., Topa, D., Roberts, A.C., Stirling, J., Raith, J.G., & Rowe, R. (2012) Eldragónite, $Cu_6BiSe_4(Se)_2$, a new mineral species from the El Dragón mine, Potosí, Bolivia, and its crystal structure. *Canadian Mineralogist* **50**, 281–294.

Paar, W.H., Brodtkorb, M.K., de Putz, H., & Martin, R.F. (2016) Atlas of Ore Minerals: Focus on Epithermal Deposits of Argentina. *Canadian Mineralogist Special Publication* **11**, 408 pp.

Pattrick, R.A.D., Coker, V.S., Pearce, C.I., Telling, N.D., & van der Laan, G. (2008) The oxidation state of copper and cobalt in carrollite, $CuCo_2S_4$. *Canadian Mineralogist* **46**, 1317–1322.

Philippo, S., Hatert, F., Bruni, Y., & Vignola, P. (2019) Luxembourgite, IMA 2018–154. CNMNC Newsletter No. 49, June 2019; *Mineralogical Magazine* **83**, 323–328.

Robinson, S.C. & Brooker, E.J. (1952) Notes and news: a cobalt–nickel–copper selenide from the Goldfields District, Saskatchewan. *American Mineralogist* **37**, 542–544.

Simon, G., Kesler, S.E., & Essene, E.J. (1997) Phase relations among selenides, sulphides, tellurides, and oxides: II. Applications to selenide-bearing ore deposits. *Economic Geology* **92**, 468–484.

Stanley, C.J., Criddle, A.J., & Lloyd, D. (1990) Precious and base metal selenide mineralization at Hope's Nose, Torquay, Devon. *Mineralogical Magazine* **54**, 485–493.

Yang, H., Hubler, D.K., Lavina, B., Downs, R.T., & Costin, G. (2007) Tyrrellite, $Cu(Co_{0.68}Ni_{0.32})_2Se_4$, isostructural with spinel. *Acta Crystallographica*, *Section C: Crystal Structure Communications* **63**, i73–i74.

Received March 22, 2019. Revised manuscript accepted May 22, 2019.